https://doi.org/10.1038/s41567-019-0440-9

nature physics

Cluster formation by acoustic forces and active fluctuations in levitated granular matter

Melody X. Lim[1,2*], Anton Souslov[1,3], Vincenzo Vitelli[1,2] and Heinrich M. Jaeger[1,2]

Mechanically agitated granular matter often serves as a prototype for exploring the rich physics associated with hard-sphere systems, with an effective temperature introduced by vibrating or shaking[1–6]. While depletion interactions drive clustering and assembly in colloids[7–10], no equivalent short-range attractions exist between macroscopic grains. Here we overcome this limitation and investigate granular cluster formation by using acoustic levitation and trapping[11–13]. Scattered sound establishes short-range attractions between small particles[14], while detuning the acoustic trap generates active fluctuations[15]. To illuminate the interplay between attractions and fluctuations, we investigate transitions among ground states of two-dimensional clusters composed of a few particles. Our main results, obtained using experiments and modelling, reveal that, in contrast to thermal colloids, in non-equilibrium granular ensembles the magnitude of active fluctuations controls not only the assembly rates but also their assembly pathways and ground-state statistics. These results open up new possibilities for non-invasively manipulating macroscopic particles, tuning their interactions and directing their assembly.

In two dimensions, particle clusters with five or fewer constituents have only one compact configuration (that is, one isostatic ground state[16]; Fig. 1a). However, beginning with six particles, there are an increasing number of energetically degenerate, but geometrically distinct, ground-state configurations. This complex energy landscape has been studied with colloids in thermal equilibrium[9,16]. Here, we explore the ground-state statistics in ensembles of macroscopic particles driven by active fluctuations that emerge from the dynamics of a driven system rather than from coupling to a heat bath. We demonstrate how energetic degeneracies, assembly rates and pathways are altered during out-of-equilibrium assembly.

To eliminate frictional interactions with container walls, we levitate particles in a sound pressure field. The same field also induces short-range, tunable nonlinear attractions that we here call acoustic forces. Not unlike depletion forces in colloids[17] or other Casimir-like forces, these acoustically mediated attractions can generate robust particle clusters. This differs from the formation of clusters in granular media due to external confinement[1,18] or, transiently, due to inelastic collisions[1,18–20]. Furthermore, the acoustic forces scale with the sound pressure amplitude, which enables precise control over cluster energetics. Such control provides advantages over cohesive forces due to capillary bridges, van der Waals interactions or charging[21,22]. Finally, in contrast to induced electric or magnetic dipole forces[23], the acoustic interactions are not aligned with an applied vector field and, due to nonlinearity, acoustic forces depend on particle motion[24].

Our set-up is illustrated in Fig. 1b. We generate a standing wave of the acoustic pressure field between an ultrasound transducer and the (transparent) acrylic reflector. Polyethylene particles (diameter 710–850 μm) levitate within a horizontal plane one-quarter of the gap height from the reflector. We image these acoustically trapped particles from the side (Fig. 1c) or from below (Fig. 1d) using a high-speed camera. When multiple particles are placed in the trap, they form compact clusters. Images of the resulting configurations for six- and seven-particle clusters are shown in Fig. 1d. Six-particle systems have three distinct ground-state configurations: parallelogram (P), chevron (C) and triangle (T). For seven-particle clusters, there are four distinct topologies: flower (Fl), tree (Tr), turtle (Tu) and boat (Bo).

Whereas colloidal clusters can be stabilized by depletion forces, acoustically levitated clusters are stabilized by in-plane acoustic forces, which are short-range pairwise[12,25] attractions generated by acoustic scattering. At close approach, these Casimir-like forces F between spherical particles scale as

$$F \sim \frac{E_0 a^6 \lambda^{-3}}{r^4} \tag{1}$$

where $E_0 \equiv \rho_0 v_0^2/2$ is the energy density of the sound field having amplitude v_0 and wavelength λ in air (density ρ_0)[26]. The particles have radius a (which enters equation (1) with a sixth power) and are distance r ($\ll \lambda$) apart. For arbitrary separation, these forces can be approximated analytically[26], or calculated in more detail with finite-element simulations using either the Gor'kov approximation[11] or fluid-structure interactions[27] (see Methods and Supplementary Information). These calculations, shown in Fig. 1e, indicate that cluster energetics are dominated by the strong short-range ($r \lesssim 0.3\lambda$) attractions between nearest neighbours, as captured in equation (1). In addition, due to the finite lateral extent of the transducer, the levitation potential exhibits a small radial gradient. However, near the centre of the trap this effect is negligibly small compared to the acoustic forces that stabilize the clusters (see Supplementary Information).

The acoustic trap can also induce non-conservative forces. Specifically, we use the fact that the particle dynamics in the acoustic field are underdamped (in contrast to colloids in a liquid) to drive instabilities that generate active fluctuations. As ref. [15] shows, a sound wave with frequency f tuned just slightly larger than the standing-wave resonance condition acts on a levitated object with a destabilizing force proportional to the object's speed. (This force depends on the frequency f, which does not enter equation (1).) As a result, the clusters fluctuate up and down in the trap, occasionally hitting the reflector. This impact transfers kinetic energy from centre-of-mass motion to modes that bend the cluster out of its planar, two-dimensional configuration. For sufficiently high

[1]James Franck Institute, The University of Chicago, Chicago, IL, USA. [2]Department of Physics, The University of Chicago, Chicago, IL, USA. [3]Department of Physics, University of Bath, Bath, UK. *e-mail: mxlim@uchicago.edu

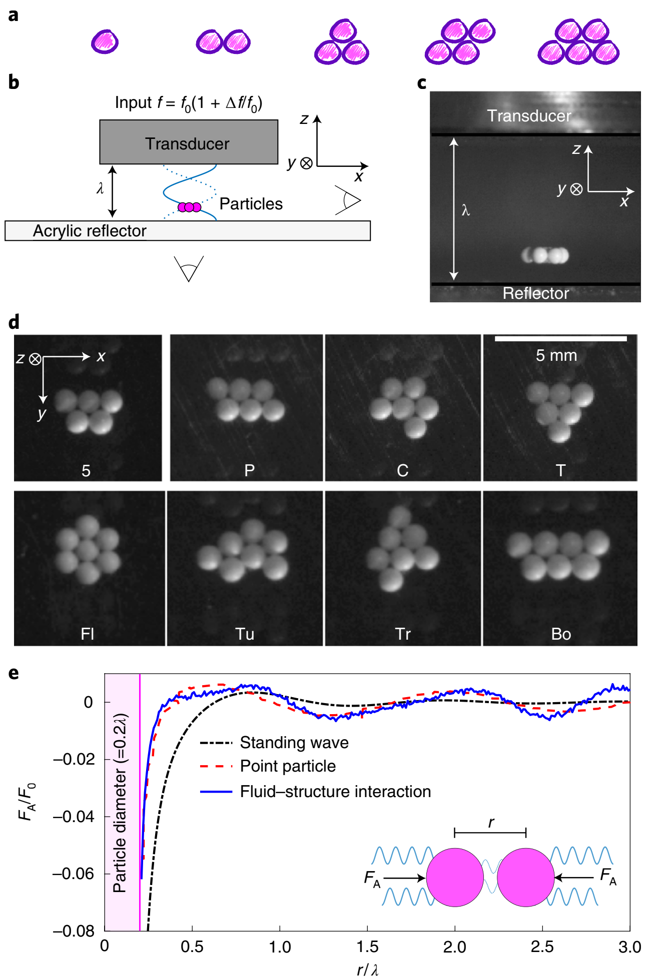

Fig. 1 | Assembling and manipulating clusters composed of macroscopic particles using acoustic levitation. a, Sketches of compact cluster configurations (isostatic ground states) for one to five particles. **b**, Schematic of the experimental set-up. An ultrasound transducer generates sound waves in air, with speed of sound $c_s = 343\,\mathrm{m\,s^{-1}}$. The distance between the transducer and the transparent acrylic reflector is chosen to create a pressure standing wave (blue line) with two nodes, at frequency $f_0 = 45.65\,\mathrm{kHz}$ and wavelength c_s/f_0. Polyethylene particles are acoustically levitated in the lower of the two nodes. **c**, Image of cluster from the side. Clusters are also imaged from below via a mirror (**d**). **d**, Different cluster configurations, imaged from below. Top: in two dimensions, there is only one five-particle cluster configuration, but six particles can form one of three distinct ground states: parallelogram P, chevron C and triangle T. Bottom: seven-particle clusters have four compact configurations: flower (Fl), turtle (Tu), tree (Tr) and boat (Bo). **e**, Inset: the scattering of the acoustic field generates short-range attractions (secondary acoustic forces) within the levitation plane, which stabilize particle clusters. Main image: force between two particles as a function of distance r between their centres, normalized by the particle weight $F_0 \equiv m_0 g$. Finite-element simulations (red dashed, blue solid lines) are compared to an analytical solution for particles in a vertical standing wave of infinite lateral extent[26] (black dashed-dotted line). See Methods and Supplementary Information for details, and Supplementary Fig. 4 for a comparison to the primary force from the confining acoustic field in a trap of finite lateral extent. Inset: schematic illustrating the secondary acoustic force due to scattering between two particles in an acoustic field.

amplitudes, these active fluctuations can lead to rearrangements between the different ground states (see Supplementary Videos 1 and 2). Finite-element simulations show that the detuning affects the magnitude of the attractive force between particles by less than 10% (see Supplementary Fig. 3 for details).

Close to resonance, six-particle clusters rearrange by ejecting a single particle, which then travels many particle diameters in a curved trajectory before it re-joins the five-particle cluster from a random angle of approach. Once the particle re-joins, it becomes stuck due to the short-range attraction. This sticky, far-from-equilibrium assembly pathway is shown in Fig. 2a. The corresponding cluster statistics retain memory of the formation process[12]: the ground-state configuration is determined by the spatial angle of approach that the sixth particle takes towards the five-particle cluster (see Supplementary Video 3). Assuming that docking onto the five-cluster is equally likely for any angle of approach (see Fig. 2a), the probabilities of forming P, C or T six-clusters are 1/2, 1/3 and 1/6, respectively, in close agreement with the data for the sticky limit (Fig. 2b).

By contrast, deep into the off-resonant regime, clusters rearrange by moving particles randomly along their periphery (Fig. 2c). This occurs either by single-particle ejection with much shorter trajectories (that is, no more than one particle diameter) or by 'floppy' hinge motions: when all but one of the bonds to nearest neighbours are broken by active cluster fluctuations, the remaining bond acts as a flexible hinge. This enables the particle to swing around to a new position without leaving the cluster. In this off-resonant regime, we find that P and C clusters occur with equal probability and twice as often as T clusters (Fig. 2b). Such cluster statistics correspond to an unbiased sampling of configuration space, where we simply count the number of ways a six-cluster can be formed by adding one more particle to a five-cluster. This ergodic limit is indistinguishable from the thermal case, which ref. [16] observed using six-particle clusters composed of micrometre-sized Brownian colloids.

By changing the ultrasound frequency, we can control the amplitude of active fluctuations and thus control the cluster rearrangement processes. Figure 2b shows statistics for relative ground-state probabilities as a function of the detuning parameter $\Delta f/f_0$, where f_0 (=45.65 kHz) is the trap resonant frequency, f is the driving frequency and $\Delta f \equiv f - f_0 > 0$. As the trap is detuned, cluster statistics transition smoothly from sticky to ergodic. At the same time, clusters increasingly rearrange via hinge motions (see Supplementary Video 4).

The emergence of hinge motions is closely linked to out-of-plane bending, which like particle ejection is triggered by impacts against the reflector, as shown in Fig. 3a (see also Supplementary Video 2). We quantify the associated deviation from the planar configuration by computing the second moment J of the vertical pixel coordinates z associated with a cluster in side view (see Methods). For a fully planar configuration, J is at a minimum; if the cluster is bent out of plane, J increases. Representative time series of J for small and large detuning parameters are shown in Fig. 3a. From longer versions of such time series, the probability distributions $P(J)$ for finding a particular magnitude J can be extracted. As Fig. 3b shows, clusters remain effectively rigid and planar for small $\Delta f/f_0$, while further detuning generates a rapidly increasing probability of exciting large-J values associated with shape-changing, out-of-plane bending fluctuations. These fluctuations also become more frequent (Fig. 3a, bottom), resulting in broad power spectra whose magnitude quickly rises with $\Delta f/f_0$, while their overall character changes little (Fig. 3c).

When we plot the average power per octave (that is, the average total power in the frequency interval from frequency f_1 to frequency $2f_1$) associated with shape-changing fluctuations we find it to increase exponentially with the detuning parameter $\Delta f/f_0$ (Fig. 3d). At the same time, we find that also the probability P_t of observing a transition between any two six-particle ground states increases exponentially (Fig. 3e). Together, these findings show that $\Delta f/f_0$ plays a role reminiscent of an effective temperature in an activated process: detuning the trap generates instabilities that temporarily break particle–particle bonds and allow for cluster rearrangement.

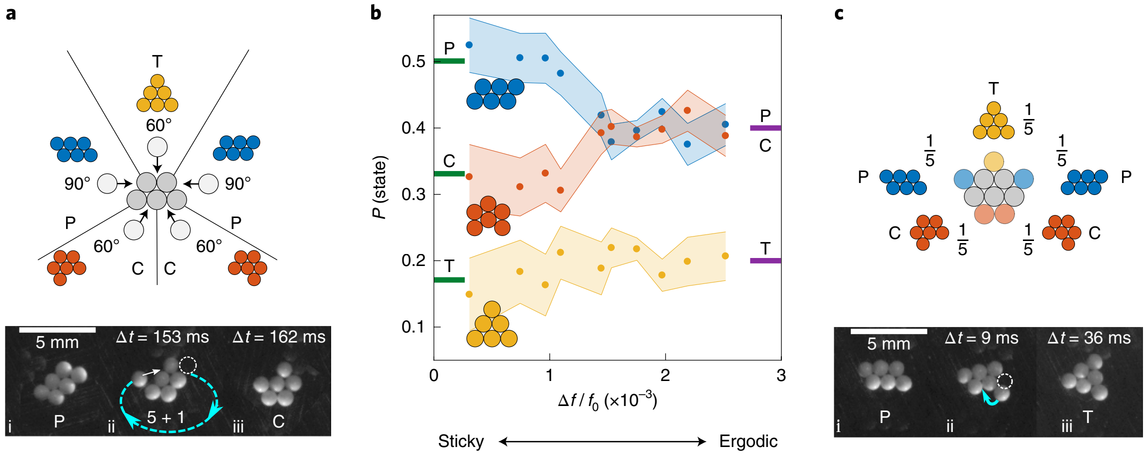

Fig. 2 | Tuning six-particle assembly between sticky and ergodic limits. Near resonance, cluster statistics follow sticky assembly (**a**). As the acoustic trap is detuned by increasing the sound frequency (**b**), cluster statistics change to ergodic assembly (**c**). **a**, Model of sticky assembly. In the regime of small detuning parameter, $\Delta f/f_0 > 0$, the likelihood of a cluster configuration is determined by the geometric angle of approach of a sixth particle to the five-particle cluster (top). Bottom: sequence of images from below showing a sticky rearrangement pathway. See Supplementary Videos 1 and 3 for dynamics. **b**, Steady-state probabilities for six-particle-cluster ground-state configurations as a function of the detuning parameter. Note that the extremes of low and high detuning parameter are well captured by the predictions of physical models from **a** and **c**, respectively. The standard error is indicated by the shaded region. The horizontal bars indicate model predictions for the sticky and ergodic limits (see the text). **c**, Model of ergodic assembly. For larger detuning, the sixth particle has equal probability of occupying each of the five binding sites on the five-particle cluster (top). Bottom: sequence of images from below showing a transition between ground states in the ergodic regime through a hinge motion. See Supplementary Videos 1 and 4 for dynamics, and Supplementary Information for the number of observations in these data.

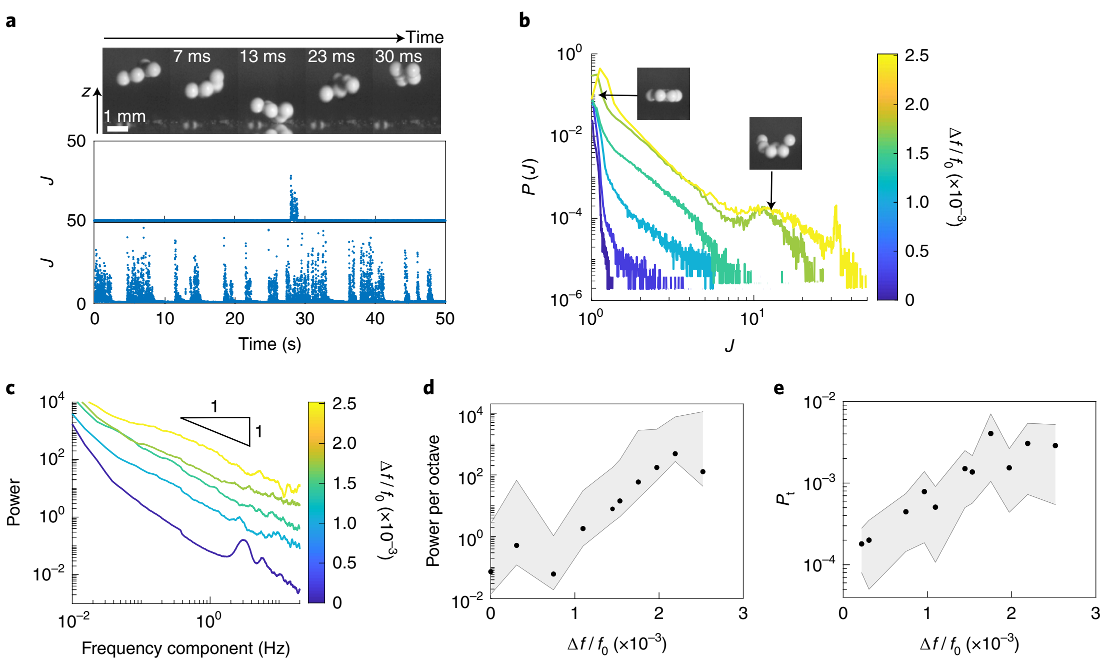

Fig. 3 | Out-of-plane motion as a measure of active fluctuations. a, Top: sequence of side images showing a cluster colliding with the reflector. See Supplementary Video 2 for dynamics. Time series for the second moment J of the vertical coordinate z (see Methods), for small detuning (middle) and large detuning (bottom). **b**, Probability distribution of J as a function of the detuning parameter, obtained from time series as in **a**. Illustrative side images of clusters are shown at their value of J. **c**, Power spectrum of the J time series. **d**, Average power per octave as a function of the detuning parameter. **e**, P_t, the probability of transition between any cluster ground state, as a function of the detuning parameter. The shaded areas in **d** and **e** indicate the standard error. Note the similar trends in **d** and **e**: the fluctuations increase exponentially as the system is detuned away from resonance.

Here, a surprising aspect is that detuning not only controls the rate, but also the type of rearrangement process. From Fig. 2b, we see that these processes have important consequences for the likelihood of observing specific ground-state configurations. In particular, the degeneracy between parallelogram (P) and chevron (C) in the ergodic limit can be broken by moving to the regime dominated by sticky assembly.

Driven by active fluctuations, these clusters explore an athermal ensemble. The cluster reconfigurations are instances of a general transition process through intermediate states. We model this process

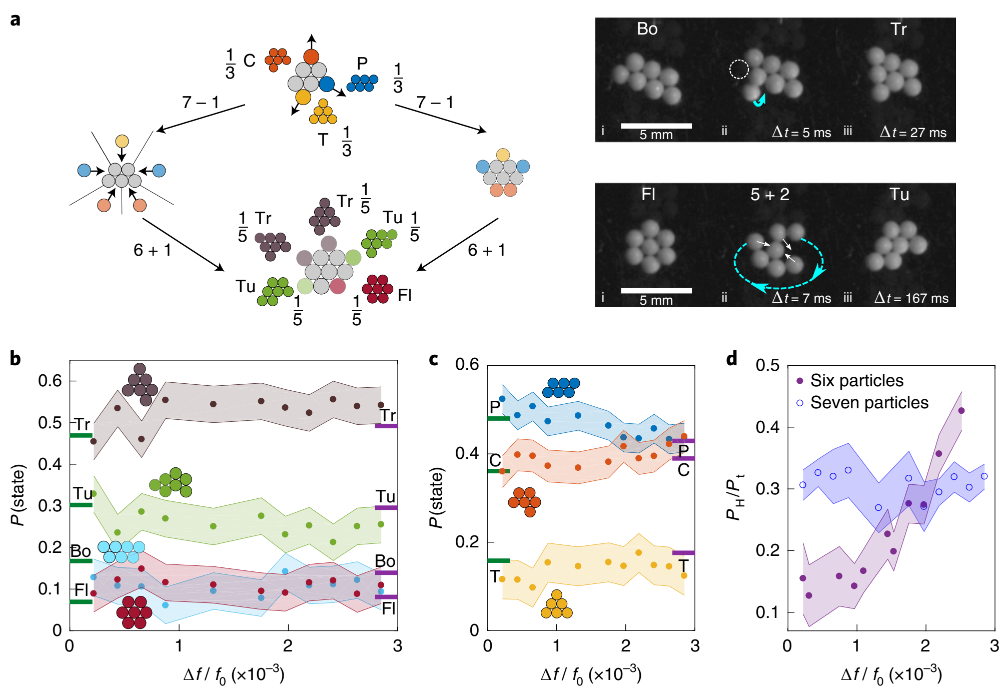

Fig. 4 | Seven-particle cluster assembly, ground-state statistics and transition states. **a**, Left: schematic of the model for statistics of six- and seven-particle clusters in the acoustic trap. The acoustic frequency tunes the formation of six-particle clusters from sticky (centre left) to ergodic (centre right) regimes. Six-particle clusters can be formed when a particle is removed from the edge of a seven-particle cluster (top). In the reverse process, seven-particle clusters are formed ergodically from six-particle clusters (bottom). Right: sequence of images from below showing a transition between seven-particle states via a hinge motion (top) or a particle ejection (bottom). See Supplementary Videos 3 and 4 for dynamics. **b**, Distribution of seven-particle cluster configurations as a function of the detuning parameter, with the standard error indicated by the shaded area. The green (purple) bars indicate statistics derived from taking into account the sticky (ergodic) six-particle clusters. **c**, Statistics of intermediate six-particle clusters within a seven-particle system, plotted as a function of the detuning parameter (standard error indicated by shaded area). The green (purple) bars indicate statistics derived from considering sticky (ergodic) cluster assembly. **d**, Probability of observing a hinge motion P_H as a fraction of the total probability of transition P_t for different values of the detuning parameter. Filled, purple (hollow, blue) discs correspond to clusters of six (seven) particles. See Supplementary Information for the number of observations in these data.

with a discrete-time Markov chain, in which state transition matrices represent the creation of specific ground-state configurations through adding or removing one particle. To represent the various ground-state probabilities P_i for a general N-particle cluster, we list them as i components of a vector $\mathbf{P}_N$. Specifically for $N=6$, $\mathbf{P}_6=(P_P, P_C, P_T)$, where the subscripts refer to the three possible configurations. The (i,j)th element of the transition matrix T_N represents the probability of creating the ith N-particle ground state by adding a single particle to the jth $(N-1)$-particle ground state. Similarly, the (i,j)th element of the matrix Q_N captures how the ith N-particle state is obtained by destroying the jth ground state of the $(N+1)$-particle cluster. Under steady-state conditions, $\mathbf{P}_N$ is related to the probabilities $\mathbf{P}_{N-1}$ and $\mathbf{P}_{N+1}$ through

$$\mathbf{P}_N = T_N\mathbf{P}_{N-1} + Q_N\mathbf{P}_{N+1} \qquad (2)$$

Once T_N and Q_N are known, equation (2) can be solved recursively for $\mathbf{P}_N$ (see Methods). For the case discussed so far, with six particles in the trap, equation (2) leads to $\mathbf{P}_6=T_6\mathbf{P}_5$ and $\mathbf{P}_5=Q_5\mathbf{P}_6$, which gives $\mathbf{P}_6=T_6Q_5\mathbf{P}_6$. Since removing any particle from a six-cluster results in the same five-cluster (so that $\mathbf{P}_5=1$), we have $Q_5=(1\ 1\ 1)$. However, the 3×1 matrix T_6 depends on whether the creation process is sticky or ergodic (that is, its components are the docking probabilities indicated in the top panels of Fig. 2a,c). Solving for $\mathbf{P}_6$ then gives the values indicated by the horizontal bars along either side of Fig. 2b, in close agreement with the data.

Having obtained T_6 and Q_5, we can now make predictions for the case that there are seven particles in the trap and $\mathbf{P}_7$ represents the four ground states shown in Fig. 1d. Figure 4a shows the reconfiguration pathways for seven-particle clusters and, as examples, transitions from boat to tree via hinge motion and from flower to turtle via particle ejection and recapture. In the model, we assume that T_7 contains only processes that generate seven- from six-particle states in an ergodic fashion. As a result, T_7 is a 4×3 matrix with elements corresponding to docking one particle at any available six-cluster site with equal probability (Fig. 4a).

Recursively solving equation (2) for $\mathbf{P}_7$, we find steady-state probabilities near 0.075, 0.47, 0.30 and 0.15 for the flower (Fl), tree (Tr), turtle (Tu) and boat (Bo) configurations (see Methods for details, and Supplementary Information for comparison to thermal seven-particle clusters). Importantly, the model indicates that all four seven-particle ground states should be largely insensitive to whether the six-particle intermediate states are formed from five-particle precursors via a sticky or ergodic process. These numerical values are in excellent agreement with the data (Fig. 4b).

A further model prediction concerns the probabilities for the intermediate six-particle states in the seven-particle system, shown in Fig. 4c. As before, these states are strongly affected by whether the sticky or ergodic assembly process is followed. However, the probabilities differ from those for the ground states in the six-particle system (Fig. 2b), since now T_7 and Q_6 enter the Markov chain model. Again we find that these probabilities are consistent with the data.

This match between model and experiments justifies, a posteriori, the above assumption about the applicability of the ergodic form of T_7 across the whole range of $\Delta f/f_0$. However, we can also check this assumption directly. This is done in Fig. 4d, where we plot the experimentally observed probability of reconfiguration via hinge motion P_H relative to P_t as a function of the detuning parameter $\Delta f/f_0$. While for six-clusters this fraction increases steadily with detuning, for seven-clusters it is effectively independent of $\Delta f/f_0$, just as the seven-cluster statistics. This difference in hinge-mode proliferation reflects that larger clusters support more bending modes and generate larger out-of-plane bending amplitudes along their periphery. We conclude that hinge motions serve as a key indicator for processes that generate ergodic reconfigurations among the ground states.

In this paper we used acoustic levitation to explore the formation and reconfiguration of small clusters of particles. While thermal fluctuations set the magnitude of depletion forces in more microscopic particle systems such as colloids, active fluctuations in the acoustic trap depend sensitively on the sound frequency. At the same time, the acoustic forces are not particularly sensitive to the sound frequency (see Supplementary Fig. 2). This allows for the control of fluctuations independently from the interactions. The cluster statistics, in turn, emerge from the dynamic response of the levitated objects to detuning the acoustic trap.

We can envision acoustic levitation as a more general platform for non-invasive manipulation of granular matter with tunable attractive interactions and further exploration of non-equilibrium assembly. Our results open up new opportunities for investigating in the underdamped regime the dynamics of extended, two-dimensional rafts of close-packed particles[28]. Since the levitated particles are macroscopic, anisotropy in acoustic forces could be achieved via particle shape and/or by combining materials with different sound-scattering properties, as demonstrated by ref. [29]. This may provide a means to assemble complex structures similar to what has been done with patchy colloids[10,30] or shape-dependent entropic forces[31]. Longer-range interactions analogous to those between particles at curved fluid interfaces[32] could be implemented using the back-action of levitated grains on the sound field itself.

Online content

Any methods, additional references, Nature Research reporting summaries, source data, statements of data availability and associated accession codes are available at https://doi.org/10.1038/s41567-019-0440-9.

Received: 10 August 2018; Accepted: 21 January 2019;
Published online: 4 March 2019

References

1. Olafsen, J. & Urbach, J. Clustering, order, and collapse in a driven granular monolayer. *Phys. Rev. Lett.* **81**, 4369–4372 (1998).
2. D'Anna, G., Mayor, P., Barrat, A., Loreto, V. & Nori, F. Observing Brownian motion in vibration-fluidized granular matter. *Nature* **424**, 909–912 (2003).
3. Feitosa, K. & Menon, N. Fluidized granular medium as an instance of the fluctuation theorem. *Phys. Rev. Lett.* **92**, 164301 (2004).
4. Keys, A. S., Abate, A. R., Glotzer, S. C. & Durian, D. J. Measurement of growing dynamical length scales and prediction of the jamming transition in a granular material. *Nat. Phys.* **3**, 260–264 (2007).
5. Komatsu, Y. & Tanaka, H. Roles of energy dissipation in a liquid–solid transition of out-of-equilibrium systems. *Phys. Rev. X* **5**, 031025 (2015).
6. Workamp, M., Ramirez, G., Daniels, K. E. & Dijksman, J. Symmetry-reversals in chiral active matter. *Soft Matter* **14**, 5572–5580 (2018).
7. Manoharan, V. N., Elsesser, M. T. & Pine, D. J. Dense packing and symmetry in small clusters of microspheres. *Science* **301**, 483–487 (2003).
8. Sacanna, S., Irvine, W. T. M., Chaikin, P. M. & Pine, D. J. Lock and key colloids. *Nature* **464**, 575–578 (2010).
9. Meng, G., Arkus, N., Brenner, M. P. & Manoharan, V. N. The free-energy landscape of clusters of attractive hard spheres. *Science* **327**, 560–563 (2010).
10. Kraft, D. J. et al. Surface roughness directed self-assembly of patchy particles into colloidal micelles. *Proc. Natl Acad. Sci. USA* **109**, 10787–10792 (2012).
11. Gorkov, L. P. Forces acting on a small particle in an acoustic field within an ideal fluid. *Sov. Phys. Doklady* **6**, 773–775 (1962).
12. Wang, M. et al. Sound-mediated stable configurations for polystyrene particles. *Phys. Rev. E* **96**, 052604 (2017).
13. Lee, V., James, N. M., Waitukaitis, S. R. & Jaeger, H. M. Collisional charging of individual submillimeter particles: using ultrasonic levitation to initiate and track charge transfer. *Phys. Rev. Mater.* **2**, 035602 (2018).
14. Settnes, M. & Bruus, H. Forces acting on a small particle in an acoustical field in a viscous fluid. *Phys. Rev. E* **85**, 016327 (2012).
15. Rudnick, J. & Barmatz, M. Oscillational instabilities in single-mode acoustic levitators. *J. Acoust. Soc. Am.* **87**, 81–92 (1990).
16. Perry, R. W., Holmes-Cerfon, M. C., Brenner, M. P. & Manoharan, V. N. Two-dimensional clusters of colloidal spheres: ground states, excited states, and structural rearrangements. *Phys. Rev. Lett.* **114**, 228301 (2015).
17. Asakura, S. & Oosawa, F. On interaction between two bodies immersed in a solution of macromolecules. *J. Chem. Phys.* **22**, 1255–1256 (1954).
18. Kudrolli, A., Wolpert, M. & Gollub, J. P. Cluster formation due to collisions in granular material. *Phys. Rev. Lett.* **78**, 1383–1386 (1997).
19. Goldhirsch, I. & Zanetti, G. Clustering instability in dissipative gases. *Phys. Rev. Lett.* **70**, 1619–1622 (1993).
20. Brilliantov, N., Saluena, C., Schwager, T. & Pöschel, T. Transient structures in a granular gas. *Phys. Rev. Lett.* **93**, 134301 (2004).
21. Royer, J. R. et al. High-speed tracking of rupture and clustering in freely falling granular streams. *Nature* **459**, 1110–1113 (2009).
22. Lee, V., Waitukaitis, S. R., Miskin, M. Z. & Jaeger, H. M. Direct observation of particle interactions and clustering in charged granular streams. *Nat. Phys.* **11**, 733–737 (2015).
23. Lumay, G. & Vandewalle, N. Controlled flow of smart powders. *Phys. Rev. E* **78**, 061302 (2008).
24. Fushimi, T., Hill, T. L., Marzo, A. & Drinkwater, B. W. Nonlinear trapping stiffness of mid-air single-axis acoustic levitators. *Appl. Phys. Lett.* **113**, 034102 (2018).
25. Zhang, S. et al. Acoustically mediated long-range interaction among multiple spherical particles exposed to a plane standing wave. *New J. Phys.* **18**, 113034 (2016).
26. Silva, G. T. & Bruus, H. Acoustic interaction forces between small particles in an ideal fluid. *Phys. Rev. E* **90**, 063007 (2014).
27. Glynne-Jones, P., Mishra, P. P., Boltryk, R. J. & Hill, M. Efficient finite element modeling of radiation forces on elastic particles of arbitrary size and geometry. *J. Acoust. Soc. Am.* **133**, 1885–1893 (2013).
28. Jambon-Puillet, E., Josserand, C. & Protière, S. Wrinkles, folds, and plasticity in granular rafts. *Phys. Rev. Mater.* **1**, 042601 (2017).
29. Owens, C. E., Shields, C. W., Cruz, D. F., Charbonneau, P. & López, G. P. Highly parallel acoustic assembly of microparticles into well-ordered colloidal crystallites. *Soft Matter* **12**, 717–728 (2016).
30. Chen, Q., Bae, S. C. & Granick, S. Directed self-assembly of a colloidal kagome lattice. *Nature* **469**, 381–384 (2011).
31. van Anders, G., Ahmed, N. K., Smith, R., Engel, M. & Glotzer, S. C. Entropically patchy particles: engineering valence through shape entropy. *ACS Nano* **8**, 931–940 (2013).
32. Cavallaro, M., Botto, L., Lewandowski, E. P., Wang, M. & Stebe, K. J. Curvature-driven capillary migration and assembly of rod-like particles. *Proc. Natl Acad. Sci. USA* **108**, 20923–20928 (2011).

Acknowledgements

We thank E. Klein and the Manoharan group for naming the seven-particle cluster configurations. We thank S. Waitukaitis, N. Schade, T. Witten, S. Nagel and R. Behringer for insightful discussions, and J. Z. Kim for a critical reading of the manuscript. This work is dedicated to the memory of R. Behringer. The research was supported by the National Science Foundation through grants DMR-1309611 and DMR-1810390. A.S. and V.V. acknowledge primary support through the Chicago MRSEC, funded by the NSF through grant DMR-1420709.

Author contributions

M.X.L. and H.M.J. conceived of the project and designed the experiments. M.X.L. performed the experiments and analysed the data. M.X.L and A.S. calculated the acoustic forces. M.X.L., A.S. and V.V. developed the model and performed the theoretical analysis. All authors contributed to writing the manuscript.

Competing interests

The authors declare no competing interests.

Additional information

Supplementary information is available for this paper at https://doi.org/10.1038/s41567-019-0440-9.

Reprints and permissions information is available at www.nature.com/reprints.

Correspondence and requests for materials should be addressed to M.X.L.

Publisher's note: Springer Nature remains neutral with regard to jurisdictional claims in published maps and institutional affiliations.

Methods

Experiment and data analysis. We used a commercial transducer (Hesentec Rank E) to generate ultrasound. An aluminium horn was bolted onto the transducer to maximize the strength of the nodes in the pressure field, following the finite-element optimization reported in ref. [33]. The base of the horn (diameter 38.1 mm) was painted black to better image the particles from below. The transducer was driven by applying an a.c. peak-to-peak voltage of 180 V, produced by a function generator (BK Precision 4052) connected to a high-voltage amplifier (A-301 HV amplifier, AA Lab Systems). Objects can be levitated stably for a range of drive amplitudes applied to the transducer. In our set-up, the amplitude can be varied from 100 to 400 V. The acrylic reflector was mounted on a lab jack and adjusted to a transducer–reflector distance λ_0, corresponding to $f_0 = 45.65$ kHz. We note that f_0 depends on the resonant frequency of the ultrasound transducer, and can thus be specified to high accuracy. Stable levitation is possible across a range of a few hertz to either side of the resonant frequency. The acoustic trap was detuned by adjusting the frequency f of the function generator. This detuning is sensitive to changes of order 10 Hz for the set-up that we use. Across the range of detuning shown in the main text, the object always returns to the nodal plane after a collision with the reflector plate. For detuning larger than 150 Hz or so, the object can no longer be levitated.

As particles we used polyethylene spheres (Cospheric, material density $\rho = 1{,}000\,\mathrm{kg\,m^{-3}}$, diameter $d = 710$–$850\,\mu$m). The particles were stored and all experiments were performed in a humidity- and temperature-controlled environment (40–50% relative humidity, 22–24 °C). The acrylic reflector was cleaned with compressed air, ethanol and deionized water before each experiment. We neutralized any charges that remained on the reflector with an anti-static device (Zerostat 3, Milty).

For each experimental run, six or seven particles were inserted into the trap using a pair of tweezers. Although clusters can be levitated in either the upper or lower of the two nodes shown in Fig. 1b, due to gravity, particles in the upper node are more easily ejected to the lower node than the other way around. Stable levitation in the lower node is therefore easier than in the upper. If clusters were levitated in the upper node, note that they would collide with the transducer rather than the reflector surface. Video was recorded using a high-speed camera (Phantom v12) at 1,000 frames per second.

To extract cluster shape information from the raw videos, we thresholded the images, then computed properties of the largest connected region in the resulting image using black-and-white image operations (regionprops). These functions are available in Matlab. Since each cluster is associated with a specific set of shape parameters, we computed the number of times a cluster shape was formed, divided by the total number of times that any cluster shape was formed, to obtain the cluster statistics in Figs. 2 and 4. Hinge motions were similarly obtained (Fig. 4). Supplementary Table S1 (S2) lists the total number of six-cluster states (seven-cluster states) observed for each value of the detuning parameter.

We calculated the second moment J of the vertical coordinate z by integrating the distance to the z geometric centre of the cluster over the area of the cluster. That is,

$$J = \iint_A (z - z_0)^2 \mathrm{d}A$$

where z_0 is the z geometric centre of the cluster. Note that we define J for the specific two-dimensional projection of the cluster side view. J is then computed similarly to the cluster topologies and hinge modes from the raw data.

Acoustic force modelling. We used finite-element modelling software (COMSOL) to model the secondary acoustic force due to scattering between a pair of particles levitated in the acoustic field (Fig. 1e), using two different methods. A schematic is shown in Supplementary Fig. 2. In both cases, we established a one-dimensional background standing pressure wave with given amplitude, such that the total pressure field P_{tot} is given by the sum of the background pressure wave and the calculated pressure. Since the background pressure wave is one-dimensional, the primary levitation force acts only in the vertical direction throughout the levitation chamber. A particle with radius $a = 0.1\lambda$ is fixed in the centre of the trap. The levitation chamber was constructed to be a cylinder of height $3\lambda_0/2$ and diameter $8\lambda_0$. In one case, labelled 'point particle' in Fig. 1e, we computed the force on a point particle in the resulting pressure field by solving the equations for the acoustic field by using the expression derived in ref. [11]. In the second case, labelled 'fluid–structure interaction' in Fig. 1e, we computed the force on a second particle of radius $r = 0.1\lambda$ by computing the full fluid–structure interaction, following the method of ref. [27].

Note that the calculations shown in Fig. 1e do not account for the finite size of the transducer, which would produce an in-plane potential gradient. In the Supplementary Information, we have performed additional calculations that account for the finite size of the transducer. These calculations create a standing wave within the geometry of the trap by applying a driving at fixed frequency to the transducer. We present these results in Supplementary Section 2 and Supplementary Fig. 4, and show that the lateral force from the finite size of the trap is very small in the region of interest near the centre of the transducer.

Markov chain model. We consider a discrete-time Markov chain that relates the cluster statistics for five-, six- and seven-particle clusters by examining the physical processes that produce different clusters. We consider the following mechanisms: seven-particle clusters are formed by ergodically adding a particle to a six-particle cluster (meaning that the particle occupies any binding site with equal probability); six-particle clusters are formed from five-particle clusters, in a way that depends on the detuning parameter; six-particle clusters are also formed from the removal of a particle from the edge of a seven-particle cluster; five-particle clusters are formed from the removal of a particle from the edge of a six-particle cluster. Denoting the probability of state S as $P(S)$, we write

$$\mathbf{P}_7 = \begin{pmatrix} P(\mathrm{Fl}) \\ P(\mathrm{Tu}) \\ P(\mathrm{Tr}) \\ P(\mathrm{Bo}) \end{pmatrix}, \mathbf{P}_6 = \begin{pmatrix} P(\mathrm{P}) \\ P(\mathrm{C}) \\ P(\mathrm{T}) \end{pmatrix}, \mathbf{P}_5 = (P(5))$$

We recall that there are four possible states for seven-particle clusters, three for six-particle clusters and one for five-particle clusters. Let $T_N^{\mathrm{e},s}$ denote the creation matrix that describes building an N-cluster from an $(N-1)$-cluster for either ergodic or sticky processes, and Q_N denote the destruction matrix for breaking an $N+1$-cluster to make an N-cluster. Then

$$\mathbf{P}_7 = T_7^{\mathrm{e}} \mathbf{P}_6 \tag{3}$$

$$\mathbf{P}_6 = \frac{1}{2} Q_6 \mathbf{P}_7 + \frac{1}{2} T_6^{\mathrm{e},s} \mathbf{P}_5 \tag{4}$$

$$\mathbf{P}_5 = Q_5 \mathbf{P}_6 \tag{5}$$

Note that we assign equal weight to the processes that form a six-particle cluster from a five-particle cluster, and those that form a six-particle cluster from a seven-particle cluster. In addition, T_6 describes either ergodic or sticky six-particle formation processes depending on the detuning parameter.

Six-particle statistics. If we exclude the seven-particle processes from the model, we are left with

$$\mathbf{P}_6 = T_6^{\mathrm{e},s} \mathbf{P}_5 \tag{6}$$

$$\mathbf{P}_5 = Q_5 \mathbf{P}_6 \tag{7}$$

We construct an effective transition matrix R_{66}, describing the six- to six-particle cluster transitions through intermediate five-particle cluster states. Substituting equation (7) into equation (6):

$$R_{66} = T_6^{\mathrm{e},s} Q_5 \tag{8}$$

To find Q_5, we consider the possible clusters that result from removing a particle from the edge of a cluster. Trivially, removing any particle from a six-cluster results in the unique five-particle cluster:

$$Q_5 = (1 \quad 1 \quad 1) \tag{9}$$

In addition, $T_6^{\mathrm{e},s}$ are constructed from the ergodic and sticky models:

$$T_6^{\mathrm{e}} = \begin{pmatrix} 2/5 \\ 2/5 \\ 1/5 \end{pmatrix}, T_6^{\mathrm{s}} = \begin{pmatrix} 1/2 \\ 1/3 \\ 1/6 \end{pmatrix} \tag{10}$$

Since the steady-state probability vector $\mathbf{P}_6$ satisfies $\mathbf{P}_6 = R_{66}\mathbf{P}_6$, we find $\mathbf{P}_6$ by finding the eigenvector of R_{66} with unit eigenvalue. For the ergodic and sticky cases respectively, we find

$$\mathbf{P}_6^{\mathrm{e}} = \begin{pmatrix} 2/5 \\ 2/5 \\ 1/5 \end{pmatrix}, \mathbf{P}_6^{\mathrm{s}} = \begin{pmatrix} 1/2 \\ 1/3 \\ 1/6 \end{pmatrix}$$

These probabilities are shown in Fig. 2b.

Seven-particle statistics. Similarly to the six-cluster derivation, we derive expressions for the effective transition matrices M_{77} and M_{66} from equations (3)–(5), such that $\mathbf{P}_7 = M_{77}\mathbf{P}_7$ and $\mathbf{P}_6 = M_{66}\mathbf{P}_6$. The steady-state probabilities are then the eigenvectors of M_{66} and M_{77} with unit eigenvalue. Note that M_{77} and M_{66} include transitions through five- and six-cluster intermediates. Substituting equations (3) and (5) into (4), we obtain

$$M_{66} = \frac{1}{2}Q_6 T_7^e + \frac{1}{2}T_6^{e,s}Q_5 \quad (11)$$

We derive M_{77} by substituting equation (5) into equation (4), which is then substituted for $\mathbf{P}_6$ in equation (3):

$$\begin{aligned}\mathbf{P}_7 &= T_7^e\left(\frac{1}{2}Q_6\mathbf{P}_7 + \frac{1}{2}T_6^{e,s}Q_5\mathbf{P}_6\right)\\ &= \frac{1}{2}T_7^e Q_6\mathbf{P}_7 + \frac{1}{2}T_7^e T_6^{e,s}Q_5\mathbf{P}_6\end{aligned}$$

To get a closed-form expression for $\mathbf{P}_7$, we continue substituting for $\mathbf{P}_6$:

$$\begin{aligned}\mathbf{P}_7 &= \tfrac{1}{2}T_7^e Q_6\mathbf{P}_7 + \tfrac{1}{2}T_7^e T_6^{e,s}Q_5\left(\tfrac{1}{2}Q_6\mathbf{P}_7 + \tfrac{1}{2}T_6^{e,s}Q_5\mathbf{P}_6\right)\\ &= \tfrac{1}{2}T_7^e Q_6\mathbf{P}_7 + \tfrac{1}{4}T_7^e T_6^{e,s}Q_5 Q_6\mathbf{P}_7\\ &\quad + \tfrac{1}{4}T_7^e T_6^{e,s}Q_5 T_6^{e,s}Q_5\mathbf{P}_6\end{aligned}$$

Continued substitution leads to a geometric series in increasing numbers of transitions between five- and six-particle cluster states:

$$\mathbf{P}_7 = \frac{1}{2}T_7^e Q_6\mathbf{P}_7 + \left(\sum_{n=1}^{\infty}\frac{1}{2^{n+1}}T_7^e(T_6^{e,s}Q_5)^n Q_6\right)\mathbf{P}_7$$

We note that $T_6^{e,s}Q_5$ is idempotent, so that $(T_6^{e,s}Q_5)^n = T_6^{e,s}Q_5$ for any n. Then we complete the geometric series and write

$$M_{77} = \frac{1}{2}T_7^e Q_6 + \frac{1}{2}T_7^e T_6^{e,s}Q_5 Q_6 \quad (12)$$

To find the destruction matrix Q_6, we assume that any particle on the edge of a cluster has equal probability to be removed. Then Fl can make only C, Tu makes P and C with equal probability, Tr makes P, C and T equally, and Bo makes only P:

$$Q_6 = \begin{pmatrix}0 & 1/3 & 1/2 & 1\\ 1 & 1/3 & 1/2 & 0\\ 0 & 1/3 & 0 & 0\end{pmatrix}$$

Similarly, we construct T_7^e assuming that a seventh particle has equal probability to attach to any binding site on a six-particle cluster:

$$T_7^e = \begin{pmatrix}0 & 1/5 & 0\\ 1/3 & 2/5 & 1\\ 1/3 & 2/5 & 0\\ 1/3 & 0 & 0\end{pmatrix}$$

Substituting into equations (11) and (12) and solving the eigenvalue problem, as for the six-particle clusters, gives

$$\mathbf{P}_7^s = \begin{pmatrix}0.071\\ 0.464\\ 0.303\\ 0.161\end{pmatrix}, \mathbf{P}_7^e = \begin{pmatrix}0.079\\ 0.480\\ 0.299\\ 0.141\end{pmatrix}$$

and

$$\mathbf{P}_6^s = \begin{pmatrix}0.484\\ 0.355\\ 0.161\end{pmatrix}, \mathbf{P}_6^e = \begin{pmatrix}0.426\\ 0.349\\ 0.180\end{pmatrix}$$

The data that support the plots within this paper and other findings of this study are available from the corresponding author upon request.

References

33. Andrade, M. A. B., Buiochi, F. & Adamowski, J. C. Finite element analysis and optimization of a single axis acoustic levitator. *IEEE Trans. Ultrason. Ferroelectr. Freq. Control* **57**, 469–479 (2010).